Coherent Nuclear Wavepacket Motions in Ultrafast Excited-State Intramolecular Proton Transfer: Sub-30-fs Resolved Pump−Probe Absorption Spectroscopy of 10-Hydroxybenzo[h]quinoline in Solution

Satoshi Takeuchi and Tahei Tahara*

Molecular Spectroscopy Laboratory, RIKEN (The Institute of Physical and Chemical Research), 2-1, Hirosawa, Wako 351-0198, Japan

Received: April 13, 2005; In Final Form: August 17, 2005

The dynamics of the excited-state intramolecular proton transfer of 10-hydroxybenzo[h]quinoline (10-HBQ) and the associated coherent nuclear motion were investigated in solution by femtosecond absorption spectroscopy. Sub-picosecond transient absorption measurements revealed spectral features of the stimulated emission and absorption of the keto excited state (the product of the reaction). The stimulated emission band appeared in the 600−800-nm region, corresponding to the wavelength region of the steady-state keto fluorescence. It showed successive temporal changes with time constants of 350 fs and 8.3 ps and then disappeared with the lifetime of the keto excited state (260 ps). The spectral feature of the stimulated emission changed in the 350-fs dynamics, which was likely assignable to the intramolecular vibrational energy redistribution in the keto excited state. The 8.3-ps change caused a spectral blue shift and was attributed to the vibrational cooling process. The excited-state absorption was observed in the 400−600-nm region, and it also showed temporal changes characterized by the 350-fs and 8.3-ps components. To examine the coherent nuclear dynamics (nuclear wavepacket motion) in excited-state 10-HBQ, we carried out pump−probe measurements of the stimulated emission and absorption signals with time resolution as good as 27 fs. The obtained data showed substantially modulated signals due to the excited-state vibrational coherence up to a delay time of several picoseconds after photoexcitation. This means that the vibrational coherence created by photoexcitation in the enol excited state is transferred to the product. Fourier transform analysis indicated that four frequency components in the 200−700-cm^{-1} region contribute to the oscillatory signal, corresponding to the coherent nuclear motions in excited-state 10-HBQ. Especially, the lowest-frequency mode at 242 cm^{-1} is dephased significantly faster than the other three modes. This observation was regarded as a manifestation that the nuclear motion of the 242-cm^{-1} mode is correlated with the structural change of the molecule associated with the reaction (the reaction coordinate). The 242-cm^{-1} mode observed in excited-state 10-HBQ was assigned to a vibration corresponding to the ground-state vibration at 243 cm^{-1} by referring to the results of resonance Raman measurements and density functional calculations. It was found that the nuclear motion of this lowest-frequency mode involves a large displacement of the OH group toward the nitrogen site as well as in-plane skeletal deformation that assists the oxygen and nitrogen atoms to come closer to each other. We discuss the importance of the nuclear wavepacket motion on a multidimensional potential-energy surface including the vibrational coordinate of the low-frequency modes.

1. Introduction

Ultrashort pulses have an energy bandwidth that is broad enough to excite a lot of vibrational eigenstates simultaneously and to generate their coherent superposition. The vibrationally coherent state thus created by photoexcitation evolves in time, which initiates the coherent nuclear motion of the molecule (the nuclear wavepacket motion).[1] Especially for molecules showing ultrafast chemical reactions in the excited state, the reaction proceeds from a photogenerated excited state that exhibits the coherent nuclear motion. Therefore, owing to the interest in possible roles of the coherence in chemical reactions, the coherence in reactive excited state has been receiving considerable attention in recent time-resolved spectroscopy using ultrashort pulses.

To consider the significance of the coherence in chemical reactions, we need to study molecules that react while the coherence is remained in the molecular system. This means that we should examine molecules that react in the femtosecond time region since the vibrational dephasing time is typically a few picoseconds in room-temperature solution. So far, typical ultrafast reactions, such as photoisomerization,[2−4] photodissociation,[5−7] proton transfer,[8−15] and electron transfer,[16−19] were investigated, and the nuclear wavepacket dynamics of these reactive molecules was discussed on the basis of the oscillatory feature observed in the time-resolved signals. For such reactions starting from a vibrationally coherent state, it is important to unveil how the coherent nuclear motion is correlated with the structural change associated with the reaction (the reaction coordinate). Recently, we studied several fundamental reactions in solution by ultrafast spectroscopy and discussed the correlation between the initial wavepacket motion and the reaction. In

* To whom correspondence should be addressed. Telephone: +81-48-467-4592. Fax: +81-48-467-4539. E-mail: tahei@riken.jp.

10.1021/jp0519013 CCC: $30.25
Published on Web 10/22/2005

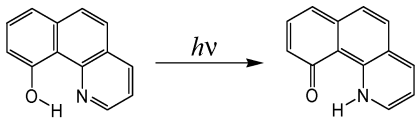

Figure 1. Intramolecular proton-transfer reaction of 10-HBQ that occurs in the photoexcited state. In this reaction, the hydroxyl proton is translocated to the benzoquinolinic nitrogen.

the photodissociation of diphenylcyclopropenone, for example, the vibrational coherence damped off in parallel with the disappearance of the precursor excited state,[7] whereas the photoisomerization of *cis*-stilbene was found to proceed after the vibrational coherence was lost within the precursor excited state.[4] The vibrational coherence in these prototypical systems was observed only in the precursor excited state, and hence, it was not transferred to the product. For better understanding of the vibrational coherence in chemical reactions, it is intriguing to study a molecular system in which the vibrational coherence is preserved throughout the reaction.

With this idea in mind, we studied another type of fundamental reactions, excited-state intramolecular proton transfer. The proton transfer is one of the simplest chemical reactions in which a proton is translocated from the donating to accepting sites. Therefore, the dephasing of the vibrational coherence is expected to be somewhat different from that in the dissociation and isomerization reactions that induce much larger structural changes. It was reported that 10-hydroxybenzo[h]quinoline (10-HBQ) exhibits the intramolecular proton transfer in the photoexcited state, and it is converted from the enol form to the keto form (Figure 1).[20] Steady-state fluorescence from the keto excited state (the product) appears in the red spectral region with the Stokes shift as large as 10000 cm^{-1}. The rise of this keto fluorescence was not yet fully time resolved in the reported femtosecond fluorescence data,[21] indicating that the proton transfer in 10-HBQ occurs in a time scale shorter than ~100 fs. As seen in Figure 1, this molecule possesses a rigid six-membered ring configuration, forming a strong intramolecular hydrogen-bonding between the hydroxyl proton and benzoquinolinic nitrogen. As a result, the photophysical properties relevant to the proton-transfer reaction are rather insensitive to solvent perturbation.[22,23] Therefore, this molecule is considered to be one of the best systems for which we can examine the vibrational coherence in the intrinsic proton-transfer process.

In this paper, we report our ultrafast absorption study of the intramolecular proton-transfer reaction of 10-HBQ in a nonpolar solvent.[24] Our sub-picosecond transient absorption measurements revealed the spectral feature of the excited-state absorption and stimulated emission due to excited-state 10-HBQ. We further examined the dynamics of these signals with time resolution as good as 27 fs and observed oscillatory feature due to the vibrational coherence. Excitation−wavelength dependence of this vibrational coherence signal was also examined, which confirmed that the oscillatory signal directly corresponds to the coherent nuclear motion. On the basis of these time-resolved data combined with frequency-domain vibrational data, we discuss the coherent nuclear dynamics and its relation to the reaction coordinate of the proton transfer.

2. Experimental Section

The experimental setup for the two-color pump−probe measurements was previously described in detail.[7] Briefly, we used two home-built noncollinear optical parametric amplifiers (NOPAs) that were driven by the output of the Ti:sapphire regenerative amplifier (CPA-1000, Clark-MXR; 1 mJ, 100 fs, 1 kHz, 840 nm). The output of the first NOPA was frequency-doubled in a thin β-BaB_2O_4 crystal, and the generated ultraviolet pulse was compressed in time by a prism pair. It was used as a pump pulse (360 or 385 nm, 17 fs) and focused into a 50-μm-thick jet stream of the sample solution. The output of the second NOPA in the visible region (<1 nJ) was divided into two, and they were used as a probe and a reference pulse for monitoring the time-resolved absorption signals. The intensities of the probe and reference pulses were detected by photodiodes, and the signals were processed on a shot-to-shot basis for the evaluation of pump-induced absorbance change. The pump polarization was rotated by a half-wave plate for the pump−probe measurements under the magic-angle condition. The time resolution of this measurement ranged from 27 to 40 fs, depending on the probe wavelength.

Transient absorption spectra were measured with sub-picosecond time resolution (380 fs) by using the same regenerative amplifier (800 nm, 100 Hz) as that employed for the two-color pump−probe measurements. The second harmonic pulse (400 nm) was used as a pump pulse for photoexcitation of the sample, whereas a white-light continuum generated by focusing the 800-nm pulse into D_2O was used as a probe and a reference pulse. The sample solution was circulated through a flow-cell with a 1-mm path length. Both the probe and reference spectra of each laser shot were analyzed by a spectrograph (500is/sm, Chromex) and detected by a CCD camera that was synchronized with the laser system. We also measured Kerr gating signals of the solvent (cyclohexane) with exactly the same experimental configuration. The obtained Kerr data were used to correct the effect of chirping of the white-light probe pulse on the time-resolved absorption data.[25]

Raman spectra were measured by using the second harmonic (405 nm) of the output of a picosecond Ti:sapphire laser (Tsunami, Spectra-Physics) and a 0.32-m spectrometer (HR-320, Jobin-Yvon) equipped with a liquid-nitrogen cooled CCD detector. A dielectric notch filter was used in front of the spectrometer to suppress the strong Rayleigh component. The frequency resolution was typically 10 cm^{-1}.

10-Hydroxybenzo[*h*]quinoline was purchased from Tokyo Kasei. It was recrystallized twice from cyclohexane and dried in vacuo before use. Spectroscopic-grade cyclohexane was received from Wako Pure Chemicals, and it was used without further purification.

Quantum chemical calculations were carried out using the Gaussian 98 package.[26] Optimized geometry and frequencies of the vibrational normal modes in the ground state were calculated using the density functional method (B3LYP) combined with the 6-311+G** basis set. The calculated frequencies were scaled by using the wavenumber-linear scaling method.[27]

3. Results and Discussion

3.1. Steady-State and Transient Absorption Spectra. The steady-state absorption spectrum of 10-HBQ in cyclohexane is shown in Figure 2A. This spectrum represents absorption of the enol form, since it is the most stable form in the electronically ground state.[20,21] The absorption spectrum shows the lowest-energy band around 380 nm due to the $S_1 \leftarrow S_0$ ($\pi\pi^*$) transition. Photoexcitation of this band generates the S_1 state of the enol form, which is the precursor of the intramolecular proton-transfer reaction. Photoexcited 10-HBQ emits fluorescence in the red spectral region, as shown by a dotted curve. This emission band was ascribed to the fluorescence from the keto excited state that is generated by the reaction (the proton-

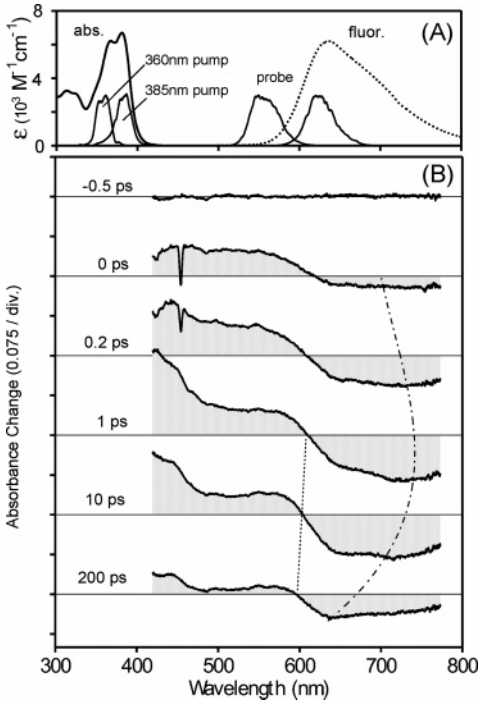

Figure 2. (A) Steady-state absorption (solid curve) and fluorescence (dotted curve) spectra of 10-HBQ in cyclohexane. The spectra of the pump and probe pulses used in the time-resolved absorption measurements with the NOPA system are also shown. (B) Transient absorption spectra of 10-HBQ in cyclohexane (1.5×10^{-2} mol dm^{-3}) measured at several delay times after photoexcitation at 400 nm. The spiky dip at 454 nm observed around the time origin is caused by the stimulated Raman gain process due to the CH stretching vibration of the solvent. The dotted and dotted−dashed curves are drawn for guides for the eye to show the spectral shifts (see text).

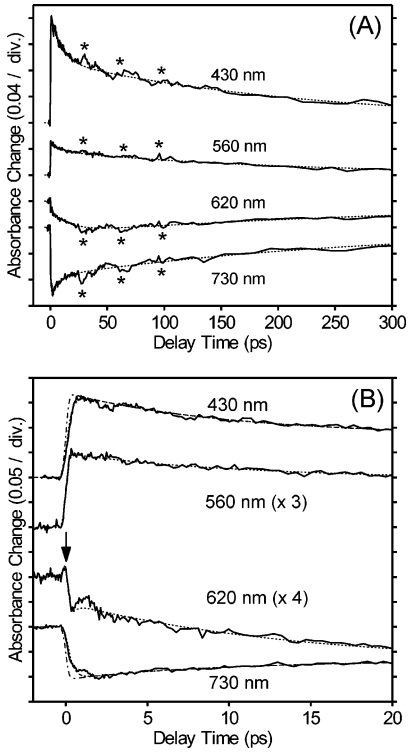

Figure 3. Temporal behavior of the transient absorption signals at four wavelengths depicted in the 0−300-ps (A) and 0−20-ps (B) time regions. The dotted curve drawn for each trace is the calculated function obtained from the fitting analysis. The dotted−dashed curves drawn for the 430- and 730-nm traces are also the calculated functions showing an instantaneous rise. The asterisk indicates experimental artifacts caused by the multiple refection of the pump pulse in the optics.

transferred product).[20] This assignment was supported by the fact that no red emission is observed in a nonproton-transfer model compound in which the hydroxyl group of 10-HBQ is replaced by the methoxy group. The observed Stokes shift as large as 10000 cm^{-1} manifests that the S_1-S_0 transition energy is substantially reduced in the keto form, indicating that the relative stability of the enol and keto forms is reversed in the excited state. Fluorescence from the initially populated S_1 state of the enol form was only observed very weakly in the reported steady-state spectrum ($\varphi \sim 8 \times 10^{-6}$),[21] because it is converted to the keto form in an ultrafast time scale.

We first measured transient absorption spectra with sub-picosecond time resolution to obtain spectral information of the excited states. Figure 2B shows transient absorption spectra of a cyclohexane solution measured at several delay times after $S_1 \leftarrow S_0$ excitation at 400 nm. Over the entire time region, the obtained spectra exhibit an absorption decrease in the wavelength region longer than ∼600 nm. Since it appears in the spectral region of the (steady-state) fluorescence, it is attributable to the stimulated emission from the keto excited state. As seen in this figure, the spectral shape of the stimulated emission band evolves in time and shows complicated dynamics: The stimulated emission first shows a rather flat band immediately after photoexcitation. Then, the relative intensity on the longer wavelength side increases as the emission grows in the sub-picosecond region. In the subsequent picosecond region, the stimulated emission apparently shows a spectral blue shift, which is manifested by the shift of the zero-crossing point around 600 nm (dotted line). On the other hand, the obtained spectra in the short wavelength region exhibit an absorption increase, i.e., the excited-state absorption. Most of this excited-state absorption is also assignable to the keto excited state, since the keto excited state is generated within the time resolution of the present measurement (380 fs). Simultaneously with photoexcitation, the excited-state absorption shows a structureless band below ∼600 nm. Then, the absorption in the 400−500-nm region builds up in the sub-picosecond region and forms a strong peak in the shorter wavelength region, although its peak wavelength could not be determined within the spectral range of the present measurement. The transient absorption spectra of 10-HBQ obtained in the present sub-picosecond measurements have revealed the spectral feature of the keto excited state generated by the proton transfer reaction. It should be noted that the transient absorption spectra measured in the present experiments are significantly different from those in a recent literature.[21] The reported spectra showed an absorption increase in the whole wavelength region of 550−750 nm, but such a spectral feature was not reproduced, not only in this sub-picosecond measurement but also in the time-resolved absorption measurement using the NOPA system described later (vide infra).

For better understanding of the complicated dynamics of excited-state 10-HBQ, we depict temporal behavior of the transient absorption signals at four selected wavelengths in Figure 3. In the 0−300-ps time scale (Figure 3A), the stimulated emission signal at 730 nm shows a biexponential decay. The decay time constants of these two components were evaluated as 8.3 ± 0.6 and 260 ± 30 ps, respectively. The longer time constant agrees very well with the reported fluorescence lifetime of the keto excited state (270 ps).[21] This ensures that the absorption decrease, which was observed in the long wavelength region of our transient absorption spectra, is due to the stimulated emission from the keto excited state. The fast component (8.3 ps) corresponds to the spectral blue shift of the

stimulated emission observed in the picosecond time region. In fact, at the short wavelength side of the stimulated emission band (620 nm), this fast component appears as a rise. It was argued that, immediately after the proton transfer, the keto excited state is formed in a vibrationally hot state with an excess energy of ~4200 cm^{-1}.[21] Therefore, the vibrational cooling process is expected to occur, in which the vibrational excess energy is dissipated to the surrounding solvent molecules. This energy dissipation process was studied with picosecond Raman spectroscopy by observing the frequency shift of a Raman band (C═C stretch of S_1 *trans*-stilbene), and it was revealed that the cooling rate of the photoexcited molecule shows a strong correlation with the thermal diffusivity of the bulk solvent.[28] We evaluated the thermal diffusivity of cyclohexane as 8.5×10^{-8} m^2 s^{-1} from its thermal conductivity (0.123 W m^{-1} K^{-1}),[29] heat capacity (156.5 J K^{-1} mol^{-1}), and density (0.7786 g cm^{-3}). By reference of the reported relation between the thermal diffusivity and the cooling rate, the evaluated thermal diffusivity of cyclohexane corresponds to the cooling rate of nearly 0.10×10^{12} s^{-1} (i.e., 10-ps cooling time). Since the observed time constant of 8.3 ps agrees very well with this estimated vibrational cooling time in cyclohexane, we can attribute this fast component to the vibrational cooling process in the keto excited state. A similar decay component (8−10 ps) was also reported in the fluorescence up-conversion study of the keto fluorescence, and it was assigned to the vibrational cooling process.[21] As seen in Figure 3A, the excited-state absorption observed in the short wavelength region (430 and 560 m) also shows a biexponential decay that consists of the 8.3- and 260-ps components. This is consistent with our assignment that the absorption increase in the 400−600-nm region is due to the absorption of the keto excited state in the picosecond time region.

Figure 3B represents the temporal behavior of the same transient absorption signals in an expanded time scale. The temporal behavior observed in this early time region varies significantly, depending on the wavelength. The excited-state absorption at 560 nm shows an "instantaneous" rise with photoexcitation, which is followed by the 8.3-ps decay (the fast component). In contrast, the transient absorption at 430 nm shows a finite rise time, corresponding to the delayed appearance of the strong absorption peak around 400 nm (Figure 2). In the fitting analysis taking account of the time resolution, we needed a single-exponential rise with a time constant of 350 ± 50 fs to reproduce the observed dynamics. This ultrafast component is also involved in the dynamics of the stimulated emission at 730 nm. As seen in the figure, the stimulated emission at 730 nm shows a finite rise time, corresponding to the spectral evolution in the long wavelength side in the sub-picosecond region. The rise at 730 nm can be reproduced fairly well by the same ultrafast component (350 fs), as shown by the dotted curve. The dynamics at 620 nm is rather complicated. The signal first shows a positive spike (indicated by arrow) around the time origin and then rapidly goes to a negative value. This behavior seems to show that an excited-state absorption signal is observed immediately after photoexcitation and is replaced, after a finite short time, by the stimulated emission from the keto excited state. Since we first photoexcited the molecule to the S_1 state of the enol form (the precursor excited state), this excited-state absorption observed only around the time origin is likely assignable to the enol excited state (before the reaction). The finite, short rise time of the stimulated emission corresponds to the proton-transfer time, although it was too short to be determined in the sub-picosecond measurement. The very similar spiky feature was also reported for other proton-transfer molecules, such as 2-(2′-hydroxyphenyl)benzoxazole[8] and 2-(2′-hydroxyphenyl)benzothiazole,[15] indicating that the absorption of the initial excited state is observed instantaneously with photoexcitation, while the stimulated emission signal appears in the overlapping spectral region after a finite time. As clearly seen in Figure 3B, the stimulated emission at 620 nm then shows a temporal change opposite to that at 730 nm: the signal at 730 nm shows the 350-fs rise and 8.3-ps decay, whereas the signal at 620 nm shows the 350-fs decay and 8.3-ps rise. This is because the wavelengths of 620 and 730 nm correspond, respectively, to the blue and red sides of the stimulated emission band, and hence, the temporal changes due to the successive spectral shifts (red shift, 350 fs; blue shift, 8.3 ps) give the opposite features at these two wavelengths. The existence of the 350-fs decay component in the stimulated emission around 620 nm was more clearly seen in the reported fluorescence up-conversion data.[21] It was also more clearly observed in time-resolved absorption measurements using the NOPA system described in the next section.

The excited-state dynamics and the corresponding spectral change of 10-HBQ can be summarized as follows based on the results of the above sub-picosecond transient absorption measurements. With photoexcitation, the excited state of the enol form is generated. The spikelike feature observed around the time origin in the 620-nm trace may be attributable to this enol excited state. This precursor state disappears very rapidly (within less than 100 fs) due to the ultrafast proton-transfer reaction. Then the keto excited state is generated, and it shows a structureless absorption band in the 400−600-nm region. The stimulated emission from the same excited state is also observed in the 600−800 nm region. The spectrum of the keto excited state shows a temporal change with the time constant of 350 fs, with which the strong absorption peak appears around 400 nm (or shorter) and the stimulated emission intensity on the longer wavelength side becomes enhanced.

The keto excited state subsequently experiences the vibrational cooling process with the time constant of 8.3 ps. During this vibrational cooling, the excited-state absorption decreases with keeping almost the same band shape, whereas the stimulated emission band shows a blue shift. This spectral blue shift of the stimulated emission is rationalized, assuming that the potential-energy surface of the keto form is shallower in the excited state than in the ground state. In this case, the "hot" fluorescence is expected to appear in the lower energy region compared to the thermally equilibrated fluorescence, because the transition from the vibrationally hot excited state occurs preferentially to the vibrationally hot ground state owing to the efficient Franck−Condon overlap.[30,31] Finally, the keto excited state decays to the ground state in the keto form with the time constant of 260 ps.

The origin of the 350-fs component was discussed previously based on the fluorescence up-conversion data.[21] Chou et al. pointed out that condensed ring systems such as 10-HBQ have two closely lying electronic excited states labeled ^1L_a and ^1L_b, and they tentatively assigned the 350-fs component to the internal conversion process between these two states in the excited keto form after the proton transfer. However, this assignment is unlikely. As we describe in the next section, we observed the coherent nuclear wavepacket motion that persists for more than a few picoseconds, and it is not reasonable that coherent nuclear motion survives in relatively slow $S_2 \rightarrow S_1$ internal conversion process. We assign this 350-fs dynamics to

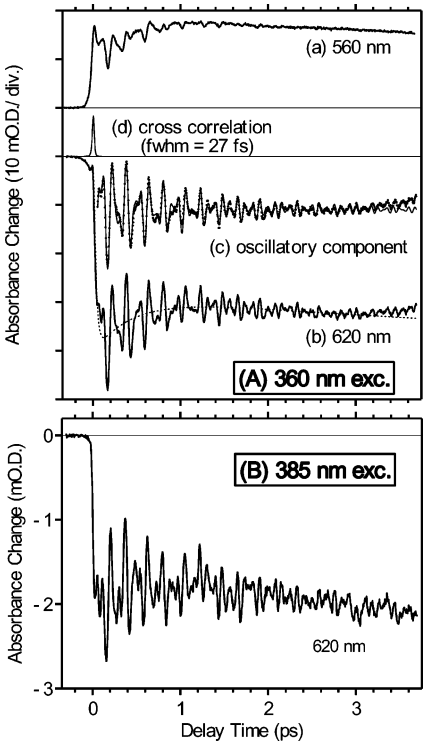

Figure 4. (A) Time-resolved absorption signals of 10-HBQ in cyclohexane (3×10^{-2} mol dm^{-3}) measured with excitation at 360 nm. The time-resolved traces were probed at 560 nm (a) and 620 nm (b), and the oscillatory component was extracted from the 620-nm trace (c). The cross correlation of the pump and probe (620 nm) pulses is also shown (d). (B) Time-resolved absorption signal at 620 nm obtained with excitation at 385 nm.

the intramolecular vibrational energy redistribution (IVR) process (see section 3.3).

3.2. Vibrational Coherence Signal and Its Excitation−Wavelength Dependence. To examine the coherent nuclear dynamics in the ultrafast proton transfer, we used the NOPA system and measured time-resolved absorption with much better time resolution (27−40 fs). Figure 4A shows time-resolved absorption signals of 10-HBQ in cyclohexane measured at two wavelengths (560 and 620 nm). These probe wavelengths correspond to the excited-state absorption and stimulated emission bands, respectively. The pump wavelength was tuned to 360 nm, which is located at the short-wavelength side of the $S_1 \leftarrow S_0$ absorption band. (The spectra of the pump and probe pulses are shown together in Figure 2A.) As readily seen in Figure 4A, we observed a substantially modulated oscillatory component due to the vibrational coherence at both probe wavelengths.

The dynamics observed in this experiment looks consistent with the transient absorption data taken with sub-picosecond time resolution (Figure 3). We observed the excited-state absorption signal at 560 nm that decays with the 8.3-ps component in this early picosecond region. Because of the improved time resolution, a spiky feature around the time origin was additionally observed, which may be assignable to the absorption of the enol excited state before the reaction. Also, a rising feature due to the 350-fs component can be seen in the 0−1-ps region, although it was not noticeable in the sub-picosecond measurement (Figure 3B). The appearance of the 350-fs rise is probably caused by the broad spectrum of the probe pulse that can cover the shorter wavelength region. (The 350-fs component was strongly observed in the 400−500-nm region.) At the probe wavelength of 620 nm, on the other hand,

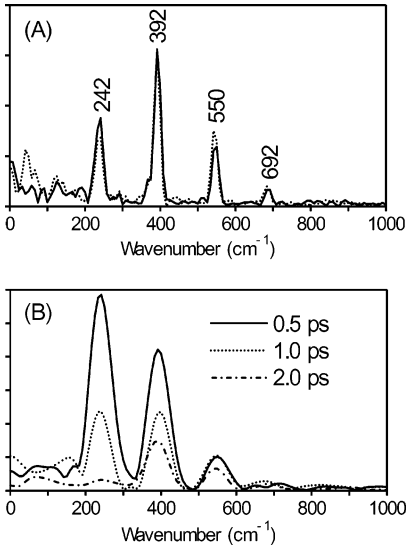

Figure 5. (A) Fourier transform spectra of the oscillatory components observed with excitation at 360 nm (solid curve) and 385 nm (dotted curve). (B) The results of the sliding-window Fourier transform with a window width of 0.5 ps. The spectra obtained by setting the window center at 0.5, 1.0, and 2.0 ps are shown together.

we observed a stimulated emission signal having a very fast rise. It decays due to the 350-fs component in the 0−1-ps region and is followed by small rising feature due to the 8.3-ps component. We simulated the observed dynamics by a multi-exponential function including the 350-fs, 8.3-ps, 260-ps, plus additional exponential rise components and optimized it to fit to the total signal. The rise time of the stimulated emission signal was evaluated as 25 ± 15 fs, which can be regarded as a measure of the proton-transfer time of 10-HBQ. The calculated function representing the intensity dynamics is also shown by dotted curves in Figure 4A.

Since the excited-state absorption and stimulated emission shown in Figure 4A are attributed to the keto excited state for almost all time except for a very short period around the time origin, the oscillatory components observed at 560 and 620 nm contain the same information about the vibrational coherence in the keto excited state. Because the oscillatory component in the stimulated emission signal is more clearly observed owing to the better time resolution at 620 nm, we further analyze the vibrational coherence in excited-state 10-HBQ only for the oscillatory component at 620 nm, in the following.

We extracted the oscillatory component by subtracting the slow intensity dynamics from the raw data (Figure 4Ac). Since the probe wavelength is far from the $S_1 \leftarrow S_0$ absorption, this oscillatory component is straightforwardly assignable to the vibrational coherence in the excited state. It is noted that the oscillation is noticeable even at the delay time of several picoseconds, which is long after the proton transfer reaction. This means that the vibrational coherence, which is initially created by photoexcitation in the excited state of the enol form, is transferred to the product and is remained in the keto excited state. This situation is apparently different from our recent observation for photoisomerization of *cis*-stilbene and photodissociation of diphenylcyclopropenone, where the vibrational coherence was only observed in the initial photoexcited state.[4,7] Fourier transform analysis showed that the extracted oscillatory signal involves at least four frequency components at 242, 392, 550, and 692 cm^{-1} (Figure 5A).

The oscillatory component arises from the temporal evolution of the vibrationally coherent state prepared by photoexcitation,

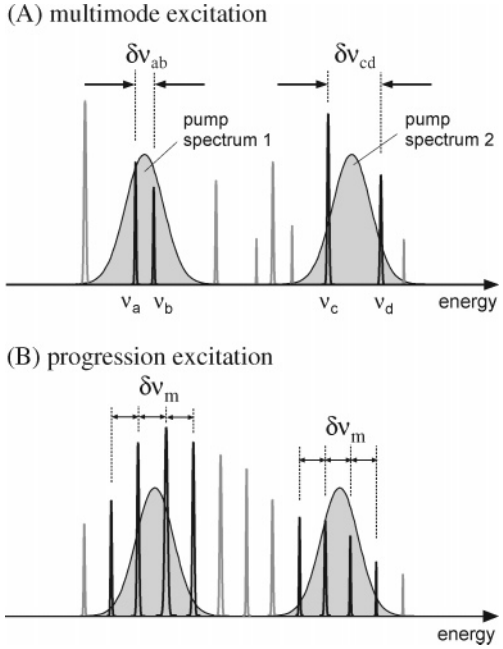

Figure 6. Schematic drawing of the vibrational lines that can be covered by two pump pulses having different center wavelengths (pump spectrum 1 and 2). (A) Multimode excitation. (B) Progression excitation.

and we often associate its frequency with that of the coherent molecular vibration straightforwardly. In general, however, the Fourier transform spectrum cannot be related directly to the frequency of the vibrational modes itself, because the period of the oscillation corresponds to the energy difference between two vibrational states that are coherently excited.[32] Accordingly, the following two mechanisms need to be considered as possible origins of the oscillatory component. The first is a coherent excitation of vibrational states that belong to different modes (the "multimode excitation", Figure 6A). In this case, the oscillation period merely corresponds to the difference frequency between the two different vibrational modes. The second is a coherent excitation of overtone/combination progression of a particular vibrational mode (the "progression excitation", Figure 6B). In this case, the oscillation period corresponds directly to the frequency of the vibrational mode, since the vibrational states in a progression appear with nearly the same energy spacing corresponding to the frequency of the vibrational mode. Obviously, it is important to distinguish these two mechanisms to further discuss the coherent nuclear dynamics based on the observed oscillatory component.

To distinguish these two mechanisms, we changed the excitation wavelength and compared the observed oscillatory signals. It is because the oscillatory component is expected to show different excitation−wavelength dependence, depending on the mechanism. In fact, when the excitation wavelength is changed, we generate another coherent superposition that consists of vibrational states in the new energy region. In the case of the multimode excitation, it is very unlikely to find a pair of vibrational states that have exactly the same energy spacing. As a result, the period of the observed oscillation should change with the change of the excitation wavelength. In the case of the progression excitation, in contrast, a pair of vibrational states with almost the same energy difference can be excited even in the new energy region, since the vibrational states in the progression are nearly equally spaced in energy. Therefore, the period of the observed oscillation does not change significantly regardless of the change of the excitation wavelength.

Figure 4B shows a time-resolved absorption signal at 620 nm obtained with 385-nm excitation. The pump pulse at 385 nm corresponds to the red edge of the $S_1 \leftarrow S_0$ absorption band (Figure 2A), and it is displaced in energy by as large as 1800 cm^{-1} from the 360-nm pump pulse. The time resolution of this measurement (28 fs) was almost the same as in the case of the 360-nm excitation. As seen in this figure, the signal shows a very similar feature to that obtained with 360-nm excitation. (The weaker signal obtained with 385-nm excitation is due to the smaller pump pulse energy.) Both of the 350-fs decay and 8.3-ps rise are noticeable also with this 385-nm excitation. The appearance of the 350-fs component even with the red-edge excitation (i.e., no excess energy) implies that this component arises from a relaxation process occurring in the keto form after the reaction. The oscillation amplitude relative to the whole signal is larger in the 385-nm data, suggesting that the vibrational coherence can be generated more efficiently by exciting the low energy region of the $S_1 \leftarrow S_0$ electronic transition.

In Figure 5A, the Fourier transform of the oscillation measured with the 360- and 385-nm excitations are compared. Obviously, both spectra exhibit four bands in the 200−700-cm^{-1} region, and more importantly, the frequency of each band coincides very well with the other. That is, the oscillation frequency did not change significantly with the change of the excitation (photon) energy by 1800 cm^{-1}. This is a clear indication that the oscillatory component arises from a coherent excitation of the overtone/combination progression relevant to each vibrational mode. It should be noted that this result is not affected substantially even if we take account of the homogeneous/inhomogeneous broadening of the vibronic transitions. Such broadening mechanisms make the vibronic structure blurred and lower the spectral selectivity given by the shift of the excitation wavelength. In the current system, however, the vibronic structure with an energy spacing of about 1000 cm^{-1} is clearly resolved in the $S_1 \leftarrow S_0$ absorption spectrum (Figure 2A). This indicates that the homogeneous/inhomogeneous broadening of the 10-HBQ/cyclohexane system is not so large as to wipe out the 1000-cm^{-1} vibronic structure. In the experiment for the excitation wavelength dependence, we shifted the excitation (photon) energy by as large as 1800 cm^{-1}, so that we can generate a new coherent superposition that is composed of essentially new vibronic states. Consequently, the above experiment for the excitation wavelength dependence can verify the mechanism for the generation of the oscillatory component, despite the inevitable influence of the homogeneous/inhomogeneous broadening in the condensed phase. Thus, we conclude that the peak frequencies in the Fourier transform spectrum directly correspond to the vibrational modes that are coherently excited.

3.3. Assignment of the Coherently Excited Vibrations. The proton-transfer reaction of 10-HBQ is initiated by photoexcitation that populates the S_1 state of the enol form (the precursor of the reaction). The photoexcitation also creates the vibrational coherence in the same precursor excited state, which induces the nuclear wavepacket motion of the vibrationally coherent state. Accordingly, the proton-transfer reaction proceeds while the nuclear motion is coherently excited. As described in the previous sections, the vibrational coherence in 10-HBQ is maintained in the course of the reaction, and hence, even the keto excited state (the product) is remained coherent. In other words, the wavepacket motion observed for the keto form is considered to contain "memory" of the nuclear motion during the ultrafast proton transfer. Therefore, for deeper understanding

of the vibrational coherence in the reaction of 10-HBQ, it is very important to discuss how the coherent nuclear motion is related to the structural change associated with the proton transfer.

Looking at the oscillatory component in Figure 4, we notice that the oscillation feature changes with time: The oscillation with a relatively long period is predominant in the early time region (0−1 ps), whereas the oscillation with a shorter period is prominent in later times. This implies that the relative amplitude of the four frequency components changes with time. To quantitatively discuss this temporal change, we performed Fourier transform analysis using a temporal window function having 0.5-ps full width at half maximum width (the "sliding-window Fourier transform"). The resultant Fourier transform spectra are shown in Figure 5B for three different delay times. It is remarkable that only the lowest-frequency mode at 242 cm^{-1} is significantly short-lived compared to the other modes. From the time dependence of the band intensity, the dephasing time of the 242-cm^{-1} mode was evaluated approximately as 0.5 ± 0.1 ps. Importantly, this dephasing time is substantially shorter than the typical vibrational dephasing time in solution (a few picoseconds), whereas the dephasing of the other modes seems ordinary and they last for as long as a few picoseconds. The significantly rapid dephasing of the 242-cm^{-1} mode suggests its particular character in this excited state.

Simply speaking, the relation between the coherent nuclear motion and the reaction coordinate can be categorized into two extreme cases, the orthogonal case and the (nearly) parallel case. In the orthogonal case, the coherent nuclear motion (nuclear wavepacket motion) occurs along a vibrational coordinate that is perpendicular to the reaction coordinate, and the motion is not coupled with the reaction. The situation of such a vibration is expected to be similar to that of ordinary vibrations in the stable state, and hence the vibration is considered to have a typical vibrational dephasing time of a few picoseconds. The dephasing time of the 242-cm^{-1} mode is obviously shorter than that expected for this orthogonal case. The lowest-frequency mode at 242 cm^{-1} seems somewhat correlated with the reaction coordinate of the proton transfer. To consider this point further, we try to make assignment of the 242-cm^{-1} mode.

Vibrational spectroscopy in the frequency domain can provide rich information for the assignment of the coherent nuclear motions. At present, however, the vibrational data such as Raman and infrared spectra are not available for excited-state 10-HBQ. Also, theoretical calculations of the excited state molecules are still a challenging task, especially for large polyatomic molecules such as 10-HBQ.[33,34] Therefore, we discuss the assignment of the 242-cm^{-1} mode by referring to the measured and calculated Raman spectra of 10-HBQ in the ground state (the enol form), which are only available at the moment. Although the excited keto form gives a major contribution to the oscillatory signal, we can expect that the skeletal vibrations are not drastically different between the keto and enol forms.

We measured a Raman spectrum of 10-HBQ in cyclohexane by using a 405-nm light (Figure 7b). Since the excitation line corresponds to the red edge of the $S_1 \leftarrow S_0$ absorption, it is (pre)resonance Raman spectrum. In the low-frequency region of this resonance Raman spectrum, we notice a band at 243 cm^{-1}, which is located very closely to the 242-cm^{-1} mode in the Fourier transform spectrum. Since the vibrational mode appearing as the oscillatory component is excited in the pumping process, it should be Franck−Condon active in the $S_1 \leftarrow S_0$ transition, i.e., a totally symmetric, Raman-active vibration.

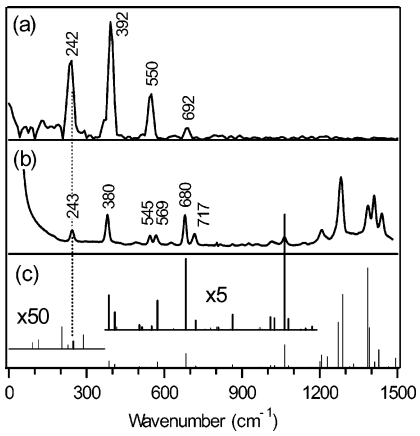

Figure 7. Comparison of the vibrational spectra of 10-HBQ. (a) Fourier transform spectrum obtained from the oscillatory component at 620 nm, (b) resonance Raman spectrum measured with 405-nm excitation, and (c) Raman spectrum in the ground state obtained by the density functional calculation. The spectra in the 0−400- and 400−1200-cm^{-1} regions are also magnified by factors of 50 and 5, respectively. In these magnified spectra, the thick lines represent totally symmetric (in-plane) vibrational modes.

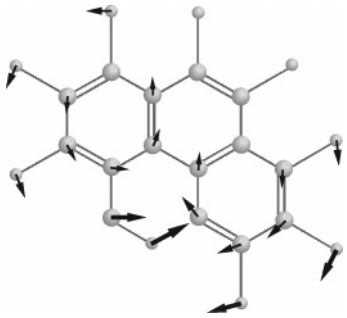

Figure 8. Nuclear motion of the ground-state vibration at 243 cm^{-1} (calculated, 248 cm^{-1}) that corresponds to the lowest-frequency wavepacket motion observed in excited-state 10-HBQ.

Thus, the corresponding vibration in the ground state is expected to be observed in the resonance Raman spectra because it is sensitive to the $S_1 \leftarrow S_0$ Franck−Condon activity (the A term resonance[35]). Therefore, the ground-state 243-cm^{-1} mode highly likely corresponds to the 242-cm^{-1} excited-state motion observed in pump−probe measurements. This assignment is consistent with a Raman spectrum calculated by the density functional method (Figure 7c). As clearly seen in the calculated spectrum, there is only one totally symmetric mode at 248 cm^{-1} in the 200−300-cm^{-1} region, and hence, it is attributable to the (ground-state) 243-cm^{-1} mode observed in the resonance Raman spectrum. From this comparison with the measured and calculated Raman spectra, we can conclude that the lowest-frequency wavepacket motion in the excited state of 10-HBQ corresponds to the in-plane vibration at 243 cm^{-1} in the ground state. We note that definitive assignment of the other three components in the Fourier transform of the excited-state oscillation (392, 550, and 692 cm^{-1}) needs further studies, such as transient Raman measurements and theoretical calculations for excited-state 10-HBQ, since there are more than one candidate in the S_0 vibrations in the vicinity of each peak frequency.

Figure 8 shows the nuclear motion of the 248-cm^{-1} (measured, 243-cm^{-1}) vibration obtained from the density functional theory calculation. In this vibrational mode, the OH group, as a whole, is displaced largely toward the nitrogen site. Since we expect the hydrogen atom to be displaced away from the oxygen atom (i.e., the lengthening of the OH distance) for the proton

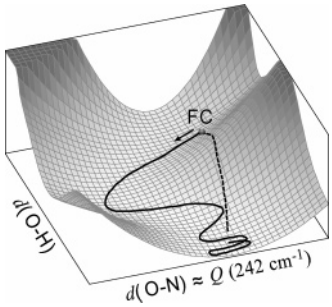

Figure 9. Schematic illustration of the potential-energy surface of excited-state 10-HBQ relevant to the proton-transfer reaction. It is drawn as a function of the O−H and O−N distances. The energetically favored trajectory from the Franck−Condon region (FC) is depicted by the solid curve, while the straight route to the final position is shown by the dashed curve.

transfer to occur, this nuclear motion does not exactly match the structural change of the proton transfer. Nevertheless, it seems that the nuclear motion in Figure 8 is closely related to the reaction. In fact, this vibration induces the displacement of the OH group and shortens the distance between the nitrogen and hydrogen atoms, which seems to make the proton transfer more feasible. In other words, the molecular skeleton of benzoquinoline deforms within the molecular plane to make the OH group to come closer to the nitrogen site. These nuclear motions look to assist the translocation of the proton. We consider that, in the overall process, the photoexcitation induces the nuclear wavepacket motion that corresponds to the mode shown in Figure 8 in the enol excited state, and the proton transfer takes place with assistance of this low-frequency deformation motion. The proton-transfer process is completed in a time as short as 25 fs, and the relevant coherent nuclear motion persists in the resultant keto excited state, which we observed. In this sense, we consider that the lowest-frequency wavepacket motion (242 cm^{-1}) in excited-state 10-HBQ is coupled with the reaction coordinate of the proton transfer.

The nuclear wavepacket motion initiated by photoexcitation seems not to point directly to the final structure (the keto form). It indicates that the wavepacket motion should be considered on the multidimensional potential surface, especially for the reaction of polyatomic molecules. In the proton transfer of 10-HBQ, we need to consider, at least, two coordinates: the vibrational coordinate of the 242-cm^{-1} mode and the proton-transfer coordinate. The 242-cm^{-1} mode is deformation of the molecular skeleton that makes the oxygen and nitrogen atoms come closer, so that this coordinate can be essentially represented by the oxygen−nitrogen distance (d(O−N)). Here, we simply represent the proton-transfer coordinate in 10-HBQ by the oxygen-proton distance (d(O−H)). We consider the wavepacket motion on this two-dimensional potential surface, as schematically illustrated in Figure 9. As seen in this illustration, the minimum-distance route of the wavepacket motion from the initial position to the final structure is not energetically favored. Instead, the wavepacket finds a more favorable route by changing the oxygen−nitrogen distance. As a result, the wavepacket is expected to show a trajectory that deviates from the minimum-distance route, which is a simple change of the O−H distance. The cooperative change of the d(O−N) and d(O−H) values is a consequence of the multidimensionality of the wavepacket motion in polyatomic molecules such as 10-HBQ. A similar multidimensional potential-energy surface was already discussed for a proton-transfer reaction of 2-(2′-hydroxy-5′-methylphenyl)-benzotriazole, where a highly anharmonic in-plane deformation mode controls the reaction dynamics by opening a barrierless transfer route on the excited-state potential.[9]

It is important to discuss the dephasing of the lowest-frequency mode at 242 cm^{-1} that shows a remarkable role in the dynamics of the proton-transfer reaction. As described above, the dephasing time of this mode was evaluated approximately as 0.5 ± 0.1 ps. This dephasing time is fairly close to the decay time constant of 350 fs recognized in the intensity dynamics. This indicates a possibility that the dephasing of the 242-cm^{-1} mode occurs in a relaxation process corresponding to the 350-fs component. A relaxation process that can lead to the vibrational dephasing is IVR. Actually, a limited number of vibrational modes are coherently excited in the pumping process, reflecting the Franck−Condon overlap in the $S_1 \leftarrow S_0$ electronic transition. Because of the ultrafast proton transfer process, the vibrational energy in excited-state 10-HBQ is expected to be rather localized within those modes even after the reaction. This localized vibrational energy then spreads to other (dark) modes through the anharmonic coupling, in which the initially excited modes can be dephased, and consequently, the statistical energy distribution to other vibrational degrees of freedom is to be realized. For excited state relevant to the reaction, the potential-energy surface is often highly anharmonic, especially along the reaction coordinate. Therefore, it is natural to think that the potential-energy surface is also anharmonic along the vibrational coordinate that is coupled with the reaction coordinate. In this sense, the lowest-frequency mode at 242 cm^{-1}, whose coordinate we consider is strongly coupled with the reaction, is expected to have an efficient anharmonic coupling with dark modes and, hence, is dephased more rapidly compared to other three modes (392, 550, and 692 cm^{-1}). The rapid dephasing due to the IVR process in the reactive excited state was recently discussed also for ultrafast proton transfer[15] and photoisomerization[4] reactions. As already mentioned, the origin of the 350-fs component was discussed previously based on the fluorescence up-conversion data,[21] and it was tentatively assigned to the internal conversion process from the ^1L_b state to ^1L_a state in the excited keto form. However, it is not natural that the internal conversion causes efficient dephasing only for a particular mode and does not affect other modes at all. It was also argued that solvent reorganization can occur even in nondipolar solvents and induce a spectral change with a sub-picosecond time scale.[36] This type of solvation arises from the interaction between the solute dipole and solvent multipole moments. The solvent used in the present study (cyclohexane) has negligibly small dipole and quadrupole moments, and it is truly a nonpolar solvent, unlike strongly quadrupolar solvents such as benzene. Consequently, it is also very unlikely that the 350-fs component is ascribed to the solvation dynamics in the nonpolar cyclohexane solution. Thus, we consider that the mode-specific dephasing observed in the present study supports the IVR process occurring in excited-state 10-HBQ with the time scale of 350 fs.

Very recently, Riedle and co-workers investigated the nuclear wavepacket dynamics in another intramolecular proton-transfer system, 2-(2′-hydroxyphenyl)benzothiazole (HBT), elaborately with similar time resolution and observed the pronounced oscillations due to the wavepacket motion in the keto excited state over the entire wavelength region of the steady-state keto fluorescence.[10,15] They analyzed the rise of the stimulated emission by a temporally delayed steplike function, which was interpreted as a manifestation of the ballistic wavepacket motion on the excited-state potential-energy surface. The evaluated delay of 33 fs corresponded to the time that the wavepacket

needs to reach the keto region along the reaction coordinate. They also presented a detailed analysis of the four oscillation components in terms of their both amplitude and phase. In particular, the lowest-frequency mode at 113 cm^{-1} was distinguished from the other three with respect to its significant fast dephasing (300 fs) as well as phase deviation from zero (vibrational turning point with the maximum displacement) at the time of the electronic configuration change to the keto form. These experimental findings and a related theoretical calculation[34] showed the importance of the wavepacket motion on a multidimensional potential-energy surface that involves not only the OH coordinate but also the vibrational coordinate of the low-frequency modes that modulates the distance between the donating (oxygen) and accepting (nitrogen) sites of the proton. In fact, they proposed a beautiful model that the wavepacket moves first to shorten the ON distance, and then when it arrives at the critical point, the electronic structure switches to induce the proton transfer from the oxygen site to the nitrogen site. Compared with their HBT, 10-HBQ possesses a rather rigid structure with its proton transfer site directly linked to the condensed ring system. Despite this difference in rigidity, the proton-transfer dynamics as well as the nuclear wavepacket dynamics relevant to the reaction looks quite similar to each other. We estimated the proton-transfer time of 10-HBQ to be 25 ± 15 fs, and it is in the same order of the proton-transfer time of HBT, although we adopted exponential functions in our analysis. More importantly, our data also suggest that the low-frequency deformational motion plays a key role in the reaction and assists the proton to be transferred. Therefore, we can consider that the involvement of the low-frequency skeletal deformation, as well as the wavepacket trajectory on the multidimensional potential-energy surface sketched,[15,34] is more or less a general feature of ultrafast intramolecular proton-transfer reaction of this kind.

Acknowledgment. We thank Professor Eberhard Riedle for stimulating discussion. S.T. acknowledges financial support by a Grant-in-Aid for Young Scientists (B) (No. 15750019) from the Ministry of Education, Culture, Sports, Science, and Technology.

References and Notes

(1) Mukamel, S. *Principles of Nonlinear Optical Spectroscopy*; Oxford University Press: New York, 1995.
(2) Szarka, A. Z.; Pugliano, N.; Hochstrasser, R. M. *Chem. Phys. Lett.* **1995**, *240*, 25.
(3) Lenderink, E.; Duppen, K.; Wiersma, D. A. *J. Phys. Chem.* **1995**, *99*, 8972.
(4) Ishii, K.; Takeuchi, S.; Tahara, T. *Chem. Phys. Lett.* **2004**, *398*, 400.
(5) Pugliano, N.; Palit, D. K.; Szarka, A. Z.; Hochstrasser, R. M. *J. Chem. Phys.* **1993**, *99*, 7273.
(6) Banin, U.; Ruhman, S. *J. Chem. Phys.* **1993**, *98*, 4391.
(7) Takeuchi, S.; Tahara, T. *J. Chem. Phys.* **2004**, *120*, 4768.
(8) Arthen-Engeland, T.; Bultmann, T.; Ernsting, N. P.; Rodriguez, M. A.; Thiel, W. *Chem. Phys.* **1992**, *163*, 43.
(9) Chudoba, C.; Riedle, E.; Pfeiffer, M.; Elsaesser, T. *Chem. Phys. Lett.* **1996**, *263*, 622.
(10) Lochbrunner, S.; Wurzer, A. J.; Riedle, E. *J. Chem. Phys.* **2000**, *112*, 10699.
(11) Wurzer, A. J.; Lochbrunner, S.; Riedle, E. *Appl. Phys. B* **2000**, *71*, 1.
(12) Ernsting, N. P.; Kovalenko, S. A.; Senyushkina, T.; Saam, J.; Farztdinov, V. *J. Phys. Chem. A* **2001**, *105*, 3443.
(13) Stock, K.; Bizjak, T.; Lochbrunner, S. *Chem. Phys. Lett.* **2002**, *354*, 409.
(14) Rini, M.; Kummrow, A.; Dreyer, J.; Nibbering, E. T. J.; Elsaesser, T. *Faraday Discuss.* **2002**, *122*, 27.
(15) Lochbrunner, S.; Wurzer, A. J.; Riedle, E. *J. Phys. Chem. A* **2003**, *107*, 10580.
(16) Wynne, K.; Reid, G. D.; Hochstrasser, R. M. *J. Chem. Phys.* **1996**, *105*, 2287.
(17) Rubtsov, I. V.; Yoshihara, K. *J. Phys. Chem. A* **1997**, *101*, 6138.
(18) Seel, M.; Engleitner, S.; Zinth, W. *Chem. Phys. Lett.* **1997**, *275*, 363.
(19) Hal, P. A.; Janssen, R. A. J.; Lanzani, G.; Cerullo, G.; Rossi, M. Z.; Silvestri, S. D. *Chem. Phys. Lett.* **2001**, *345*, 33.
(20) Martinez, M. L.; Cooper, W. C.; Chou, P. T. *Chem. Phys. Lett.* **1992**, *193*, 151.
(21) Chou, P. T.; Chen, Y. C.; Yu, W. S.; Chou, Y. H.; Wei, C. Y.; Cheng, Y. M. *J. Phys. Chem. A* **2001**, *105*, 1731.
(22) Chou, P. T.; Wei, C. Y. *J. Phys. Chem.* **1996**, *100*, 17059.
(23) Chou, P. T.; Wu, G. R.; Liu, Y. I.; Yu, W. S.; Chiou, C. S. *J. Phys. Chem. A* **2002**, *106*, 5967.
(24) Takeuchi, S.; Tahara, T. *Femtochemistry and Femtobiology: Ultrafast Events in Molecular Science*; Martin, M. M., Hynes, J. T., Eds.; Elsevier: The Netherlands, 2004; p 295.
(25) Yamaguchi, S.; Hamaguchi, H. *Appl. Spectrosc.* **1995**, *49*, 1513.
(26) Frisch, M. J.; Trucks, G. W.; Schlegel, H. B.; Scuseria, G. E.; Robb, M. A.; Cheeseman, J. R.; Zakrzewski, V. G.; Montgomery, J. A., Jr.; Stratmann, R. E.; Burant, J. C.; Dapprich, S.; Millam, J. M.; Daniels, A. D.; Kudin, K. N.; Strain, M. C.; Farkas, O.; Tomasi, J.; Barone, V.; Cossi, M.; Cammi, R.; Mennucci, B.; Pomelli, C.; Adamo, C.; Clifford, S.; Ochterski, J.; Petersson, G. A.; Ayala, P. Y.; Cui, Q.; Morokuma, K.; Malick, D. K.; Rabuck, A. D.; Raghavachari, K.; Foresman, J. B.; Cioslowski, J.; Ortiz, J. V.; Stefanov, B. B.; Liu, G.; Liashenko, A.; Piskorz, P.; Komaromi, I.; Gomperts, R.; Martin, R. L.; Fox, D. J.; Keith, T.; Al-Laham, M. A.; Peng, C. Y.; Nanayakkara, A.; Gonzalez, C.; Challacombe, M.; Gill, P. M. W.; Johnson, B. G.; Chen, W.; Wong, M. W.; Andres, J. L.; Head-Gordon, M.; Replogle, E. S.; Pople, J. A. *Gaussian 98*, revision A.11; Gaussian, Inc.: Pittsburgh, PA, 1998.
(27) Yoshida, H.; Ehara, A.; Matsuura, H. *Chem. Phys. Lett.* **2000**, *325*, 477.
(28) Iwata, K.; Hamaguchi, H. *J. Phys. Chem. A* **1997**, *101*, 632.
(29) Hirata, Y.; Okada, T. *Chem. Phys. Lett.* **1991**, *187*, 203.
(30) Sarkar, N.; Takeuchi, S.; Tahara, T. *J. Phys. Chem. A* **1999**, *103*, 4808.
(31) Tahara, T. In *Advances in Multi-Photon Processes and Spectroscopy*; Lin S. H., Villaeys A. A., Fujimura Y., Eds.; World Scientific: 2004; Vol. 16, Chapter 1.
(32) Takeuchi, S.; Tahara, T. *Chem. Phys. Lett.* **2000**, *326*, 430.
(33) Sobolewski, A. L.; Domcke, W. *Phys. Chem. Chem. Phys.* **1999**, *1*, 3065.
(34) Vivie-Riedle, R.; Waele, V. D.; Kurtz, L.; Riedle, E. *J. Phys. Chem. A* **2003**, *107*, 10591.
(35) Albrecht, A. C. *J. Chem. Phys.* **1961**, *34*, 1476.
(36) Reynolds, L.; Gardecki, J. A.; Frankland, S. J. V.; Horng, M. L.; Maroncelli, M. *J. Phys. Chem.* **1996**, *100*, 10337.